Surface and shear horizontal waves in piezoelectric composites

G. Monsivais,[1] J. A. Otero,[2,3] and H. Calás[3]
[1]*Instituto de Física, Universidad Nacional Autónoma de México, Apartado Postal 20-364, 01000 Mexico D.F., Mexico*
[2]*Instituto Tecnológico y de Estudios Superiores de Monterrey, Apartado Postal 18, Atizapan, Edo. de Mexico, Mexico*
[3]*Instituto de Cibernética, Matemática y Física (ICIMAF), Calle 15 e/t C y D. CP 10400, Vedado, Habana 4, Cuba*
(Received 23 June 2004; published 1 February 2005)

Surface and shear horizontal waves in piezoelectric composite media consisting of piezoelectric layers of hexagonal 6*mm* symmetry are studied. We consider finite and infinite systems. For the finite case we study "periodic" and two types of nonperiodic structures: Fibonacci sequences and systems with a linear perturbation in the piezoelectric parameters which give rise to resonances of Stark-Ladder type. For the infinite case we only consider periodic systems. The transmission, dispersion relation, angular dispersion relation, and eigenmodes of vibration of the composites are analyzed. We discuss in detail the effect of surface waves on these properties. We use the transfer matrix formalisms of 4×4 and 2×2 dimensions to study the system in the exact approach and in the approximation where the surface waves are neglected, respectively. Numerical results are also presented.

DOI: 10.1103/PhysRevB.71.064101 PACS number(s): 77.65.Fs, 77.65.Dq, 77.90.+k

I. INTRODUCTION

Due to increasing implementation of acoustoelectronic devices in modern communication systems, the study of acoustic wave propagation in solid structures has received much attention in recent years. Layered composites may support novel types of waves with specific frequency dependence of phase and group velocities that do not exist on homogeneous substrates.

There are two kinds of wave motion in elementary physics: traveling waves, which can have any frequency, and standing waves, which occur only for discrete "allowed" frequencies. But there exists a third kind of wave motion that occurs in periodic media. In this case the frequency spectrum shows a band structure, that is, the allowed frequencies fall into continuous "bands," separated by forbidden "gaps." In the quantum context there is a similar behavior of the energy spectrum of the electrons in periodic potentials. This was clearly shown by Kronig and Penney in the classic paper that laid the foundation for the modern theory of solids.[1] Band structure is practically the signature of solid state physics, but the same phenomenon occurs, in principle, for mechanical, acoustical, electromagnetic, and even oceanographic waves.

One of the most effective theoretical tools for the exact analytical study of various wave phenomena in periodically stratified media is the method of the propagator matrix based on the Bloch formalism. However, the direct analytical calculations become very cumbersome once the dimension of the propagator matrix is higher than 2×2 due to the coupled-mode effect. It occurs, for instance, at a mixing of the sagittal acoustic modes in a symmetry plane of purely elastic stratified media[2–6] or at the shear horizontal (SH) waves propagation in the presence of electromechanical coupling.[2,7–11]

Theoretical treatment in those cases is largely numerical. The explicit analytical results have been mainly confined to obtaining the Bloch dispersion relation (the characteristic equation for the propagator matrix), whereas the direct analytical calculation of the relation itself has been discussed under certain fairly restrictive approximations and assumptions. For example, in particular, in Refs. 10 and 11 the propagator matrix has been effectively reduced to the 2×2 dimension thanks to the screening properties of metallized interfaces separating piezoelectric layers. The analytical method, which has been worked out in Ref. 6 for solid layers, assumes a semi-infinite periodic structure and a normal incidence. The reflection coefficient[6] was obtained in a somewhat implicit form, via the root of a matrix equation.

In the present paper, we analyze finite and infinite piezoelectric laminated composites. For the finite case we consider "periodic" and two types of nonperiodic systems: Fibonacci chains and structures with a linear variation of the piezoelectric parameters as a function of the distance along the axis of the piezocomposite. This configuration gives rise to the Stark-Ladder resonances (SLR). In these cases we study the scattering of incident SH and surface piezoelectric waves as a function of the material properties, width of the layers, angle of incidence, and frequency. For the infinite case we only consider periodic systems and we analyze the dispersion relation, angular dispersion relation (as defined below), and eigenmodes of vibration. We also consider the case when a polymer bonding layer of araldite is placed between each couple of piezoelectric layers. In all cases we discuss in detail the effects of the surface waves. These waves are sometimes neglected in order to simplify the calculations (see, for example, Ref. 12). These approximated calculations will be referred as the *non-surface wave approximation* (NSWA).

This work is devoted to the study of wave propagation in solid multilayered piezoelectric systems which can be in contact with other solids. The problem involving interaction with fluids is studied in other works[13,14] and it is not considered in this paper. The study and the applications of different piezoelectric layered structures have been facilitated by the development of the computationally efficient transfer matrix method for certain types of matrix.[15–17] However, the description of the surface waves by means of the transfer matrix requires exponential functions of real argument (as we

 ©2005 The American Physical Society

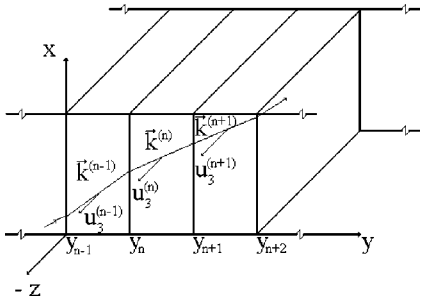

FIG. 1. Layers of the piezocomposite with their interfaces at $y_{n-1}, y_n, y_{n+1}, y_{n+2}$, etc. The wave vector in the nth layer is $\mathbf{k}^{(n)}$ with magnitude $k^{(n)}=|\mathbf{k}^{(n)}|=\sqrt{\rho^{(n)}\omega^2/c_{44}^{(n)}}$ and the mechanical displacement in the z direction is $u_3^{(n)}(x,y,t)$.

will see below), and therefore the numerical calculations become unstable for large multilayered media.[18] So, more appropriate methods have been developed, for example: surface impedance method,[19–26] global matrix method,[27–30] etc. However, these methods are time-consuming and it is important to have an idea of how much the results are modified when surface waves are neglected to avoid numerical instabilities. Thus in this paper the surface waves are included in the formalism and the results are compared with those of the NSWA.

II. STATEMENT OF THE PROBLEM

The piezoelectric materials that will be considered in this paper have been the object of many studies since 1969 when Bleustein and Gulyaev simultaneously discovered that in these systems there exists a SH wave. This is known today as the Bleustein-Gulyaev wave.[31–33]

Thus let us consider a SH piezoelectric wave which is traveling inside a layered heterogeneous piezoelectric medium with crystal symmetry class 6*mm* whose six-order symmetry axis coincides with the z axis ($z=x_3$). The OY axis was chosen perpendicular to the interfaces. Let us assume the SH wave propagates in the XY plane ($x=x_1, y=x_2$), and it is polarized along the OZ axis (see Fig. 1). It will be shown in Sec. IV that the system admits, in fact, this kind of wave propagation. We define the nth layer as the layer between the coordinates y_n and y_{n+1}. The thickness of the nth layer is p_n. The wave vector of the traveling wave inside the nth layer will be denoted by $\mathbf{k}^{(n)}$ and its components on the OX, OY, OZ axes by $k_x^{(n)}$, $k_y^{(n)}$, $k_z^{(n)}=0$, respectively. The wave number is $k^{(n)}=|\mathbf{k}^{(n)}|$. As mentioned, we will consider finite and infinite systems. For the first case we will assume that the composite is embedded within two semi-infinite piezoelectric media, one of them located on the left and the other on the right. In this case the piezocomposite is made of N piezoelectric layers which are inside the two semi-infinite media. The layers associated with the values $n=-1$ and $n=N$ are the left semi-infinite medium and the right semi-infinite medium, respectively, thus $-1\leqslant n\leqslant N$. The interface between the left (right) semi-infinite medium and the system is at $y=y_0=0$ ($y=y_N$). We will analyze the response of the layered piezocomposite when the waves impinge at an angle θ from the left semi-infinite medium upon the system.

Both for finite and infinite cases we will be interested first in periodic structures. However, as mentioned, two nonperiodic special structures will be also considered. For the first case "periodic structure" means n_p periods in the interval $[y_0, y_N]$ in such a way that the piezocomposite consists of a set of n_c layers repeated n_p times and therefore $N=n_c\cdot n_p$. The n_c layers are made, in general, of different piezoelectric homogeneous materials. We will describe the macroscopic properties of the nth layer by means of the following quantities: the tensor of elastic moduli $c_{ijkl}^{(n)}$, the tensor of piezoelectric moduli $e_{kij}^{(n)}$, the dielectric tensor $\varepsilon_{ij}^{(n)}$, and the density $\rho^{(n)}$.

The system described above will be studied using the continuum mechanics approach with the quasistatic approximation for the electric potential.

III. FUNDAMENTAL EQUATIONS OF PIEZOELECTRICITY

Since the layers are made of homogeneous material, we can use in each layer the dynamic equations of elasticity (for simplicity we will omit in this section the index n):

$$\frac{\partial \sigma_{ij}}{\partial x_j}=\rho\frac{\partial^2 u_i}{\partial t^2},\quad i,j=1,2,3, \tag{1}$$

which describe the wave propagation in piezoelectric crystals.[34,35] The components of the stress tensor σ_{ij} are related with the strain tensor components S_{kl} and with the electric field E_k components by means of

$$\sigma_{ij}=c_{ijkl}S_{kl}-e_{kij}E_k,\quad i,j,k,l=1,2,3, \tag{2}$$

where

$$S_{kl}=\frac{1}{2}\left(\frac{\partial u_k}{\partial x_l}+\frac{\partial u_l}{\partial x_k}\right), \tag{3}$$

u_1, u_2, u_3 being the components of the mechanical displacement vector $\mathbf{u}$.

Together with Eq. (1) we need the Gauss law[34,35]

$$\frac{\partial \boldsymbol{D}_i}{\partial x_i}=0, \tag{4}$$

where $\boldsymbol{D}_i$ is the ith component of the electric displacement vector given by

$$\boldsymbol{D}_i=e_{ikl}S_{kl}+\varepsilon_{ij}E_j. \tag{5}$$

Furthermore, in the quasistatic approximation we have $E_j=-\partial\phi/\partial x_j$, where ϕ is the electric potential.

Taking into account Eq. (3) and substituting Eqs. (2) and (5) into Eqs. (1) and (4), we obtain the following system of equations:

$$c_{ijkl}\frac{\partial^2 u_k}{\partial x_l\partial x_j}+e_{kij}\frac{\partial^2\phi}{\partial x_k\partial x_j}=\rho\frac{\partial^2 u_i}{\partial t^2},$$

$$e_{ikl}\frac{\partial^2 u_k}{\partial x_l\partial x_i}-\varepsilon_{ik}\frac{\partial^2\phi}{\partial x_k\partial x_i}=0. \tag{6}$$

IV. METHOD OF SOLUTION

For piezoelectric materials of class 6*mm* the system of Eqs. (6) can be separated in two systems of differential equations corresponding to the shear vertical (SV) and SH waves respectively.[34,35] The SH waves correspond to a nontrivial solution of the system with $u_3 \neq 0$, $\phi \neq 0$ both independent of z and $u_1 = u_2 = 0$. Under these considerations the system becomes

$$c_{44}\left(\frac{\partial^2 u_3}{\partial x^2} + \frac{\partial^2 u_3}{\partial y^2}\right) + e_{15}\left(\frac{\partial^2 \phi}{\partial x^2} + \frac{\partial^2 \phi}{\partial y^2}\right) = \rho \frac{\partial^2 u_3}{\partial t^2}, \tag{7}$$

$$e_{15}\left(\frac{\partial^2 u_3}{\partial x^2} + \frac{\partial^2 u_3}{\partial y^2}\right) - \varepsilon_{11}\left(\frac{\partial^2 \phi}{\partial x^2} + \frac{\partial^2 \phi}{\partial y^2}\right) = 0, \tag{8}$$

where we are using an abbreviated notation for c_{ijkl} and e_{ikl} which assigns a single index α to the couple ij and a single index β to the couple kl according to the rule

$$\begin{bmatrix} 11 & 12 & 13 \\ 21 & 22 & 23 \\ 31 & 32 & 33 \end{bmatrix} \rightarrow \begin{bmatrix} 1 & 6 & 5 \\ 6 & 2 & 4 \\ 5 & 4 & 3 \end{bmatrix}. \tag{9}$$

The system (7) and (8) has the following four nontrivial linearly independent solutions:[36]

$$\phi(x,y,t) = \exp[i(k_x x + k_y y - \omega t)]$$

$$\text{with } u_3(x,y,t) = \frac{\varepsilon_{11}}{e_{15}}\phi(x,y,t), \tag{10}$$

$$\phi(x,y,t) = \exp[i(k_x x - k_y y - \omega t)]$$

$$\text{with } u_3(x,y,t) = \frac{\varepsilon_{11}}{e_{15}}\phi(x,y,t), \tag{11}$$

$$\phi(x,y,t) = \exp[i(k_x x - \omega t) + k_x(y - y_n)]$$

$$\text{with } u_3(x,y,t) = 0, \tag{12}$$

$$\phi(x,y,t) = \exp[i(k_x x - \omega t) - k_x(y - y_n)]$$

$$\text{with } u_3(x,y,t) = 0, \tag{13}$$

where

$$k_y^2 = \frac{\rho\omega^2}{\overline{c}_{44}} - k_x^2 = k^2 - k_x^2 = k^2 \cos^2\theta, \tag{14}$$

$$\overline{c}_{44} = c_{44} + \frac{e_{15}^2}{\varepsilon_{11}}, \tag{15}$$

θ being the angle of incidence. The general solution to Eqs. (7) and (8) at the nth layer is a linear combination of the four particular solutions given in expressions (10)–(13) as follows:

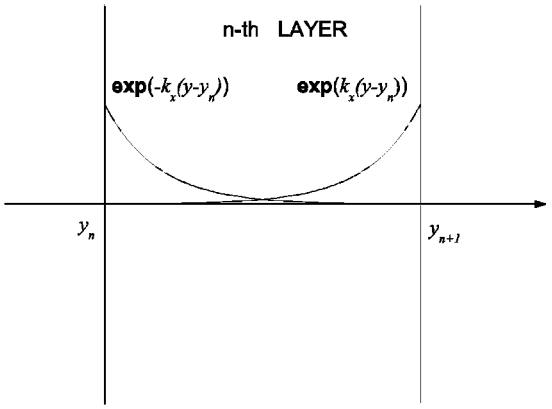

FIG. 2. The surface waves in the nth layer are described by exponential functions $\exp[k_x(y-y_n)]$ and $\exp[-k_x(y-y_n)]$ of real argument and they are localized around the y_n and y_{n+1} coordinates, respectively.

$$u_3^{(n)}(x,y,t) = \frac{\varepsilon_{11}^{(n)}}{e_{15}^{(n)}}(A^{(n)} \exp[ik_y^{(n)} y] + B^{(n)} \exp[-ik_y^{(n)} y])\exp[i(k_x x - \omega t)], \tag{16}$$

$$\phi^{(n)}(x,y,t) = \frac{e_{15}^{(n)}}{\varepsilon_{11}^{(n)}} u_3^{(n)}(x,y,z) + \{C^{(n)} \exp[k_x(y - y_n)] + D^{(n)} \exp[-k_x(y - y_n)]\}\exp[i(k_x x - \omega t)], \tag{17}$$

where $A^{(n)}$, $B^{(n)}$, $C^{(n)}$, and $D^{(n)}$ are coefficients that will be determined below. The wave vector k_x is the same in all layers due to the Snell law and therefore it does not have a label n.

We see that the electric potential $\phi^{(n)}(x,y,t)$ is a linear combination of two parts, one part (referred to as $\Phi_{md}^{(n)} \times (x,y,t) \equiv \overline{\Phi}_{md}^{(n)}(y)\exp[i(k_x x - \omega t)]$) is proportional to the mechanical displacements $u_3^{(n)}(x,y,z)$ and the other part (referred to as $\Phi_{sw}^{(n)}(x,y,t) \equiv \overline{\Phi}_{sw}^{(n)}(y)\exp[i(k_x x - \omega t)]$) represents the surface waves[36–38] of the nth layer "located" at the interfaces $y = y_n$ and $y = y_{n+1}$ (see Fig. 2). Furthermore, for layers of hexagonal 6*mm* symmetry we have, from Eqs. (3), (5), (10), (11), and (17),

$$\boldsymbol{D}_2^{(n)}(x,y,t) = -\varepsilon_{11}\frac{\partial \overline{\Phi}_{sw}^{(n)}}{\partial y} = -\varepsilon_{11} k_x \{C^{(n)} \exp[k_x(y - y_n)] - D^{(n)} \exp[-k_x(y - y_n)]\}\exp[i(k_x x - \omega t)]. \tag{18}$$

Thus the electric displacement $\boldsymbol{D}_2^{(n)}$ (as well as $\Phi_{sw}^{(n)}$) only involves surface waves. In the NSWA we will take $C^{(n)}$ and $D^{(n)}$ equal to zero. Therefore $\Phi_{sw}^{(n)} = D_2^{(n)} = 0$ and $u_3^{(n)} = (\varepsilon_{11}^{(n)}/e_{15}^{(n)})\Phi_{md}^{(n)} = (\varepsilon_{11}^{(n)}/e_{15}^{(n)})\phi^{(n)}$. In this case only the first 2×2 block of the 4×4 transfer matrices discussed in the next sections will be used.

In order to have the complete solution for the whole system and to determine unambiguously the coefficients $A^{(n)}$, $B^{(n)}$, $C^{(n)}$, and $D^{(n)}$ we need to find the relation between the solution at a given layer and the solutions at its neighboring layers. This is done by using the boundary conditions (BC). These can be summarized in two groups: the conditions acting at each interface, and those related with the global characteristics of the solution (for finite systems the global characteristics are direction of the incident wave, bound solutions, etc., and for infinite systems the global characteristic is the Bloch condition).

A. BC at the interfaces and their implications

For the first group, we consider at each interface the continuity of the displacement u_3, the stress tensor σ_{23}, the electric displacement $\boldsymbol{D}_2$, and the electric potential ϕ. These conditions can be written in the following form:

$$u_3^{(n)}(y_n) = u_3^{(n-1)}(y_n), \tag{19}$$

$$\sigma_{23}^{(n)}(y_n) = \sigma_{23}^{(n-1)}(y_n), \tag{20}$$

$$\boldsymbol{D}_2^{(n)}(y_n) = \boldsymbol{D}_2^{(n-1)}(y_n), \tag{21}$$

$$\phi^{(n)}(y_n) = \phi^{(n-1)}(y_n). \tag{22}$$

Using conditions (19)–(22) we obtain the transfer matrix denoted by $\mathbf{M}^{(n-1,n)}$, which relates the coefficients $A^{(n)}$, $B^{(n)}$, $C^{(n)}$, and $D^{(n)}$ defined in Eqs. (16) and (17) associated with the solution at the nth layer with the corresponding coefficients $A^{(n-1)}$, $B^{(n-1)}$, $C^{(n-1)}$, and $D^{(n-1)}$ associated with the solution at the $(n-1)$th layer by means of the expression

$$\begin{pmatrix} A^{(n)} \\ B^{(n)} \\ C^{(n)} \\ D^{(n)} \end{pmatrix} = \mathbf{M}^{(n-1,n)} \begin{pmatrix} A^{(n-1)} \\ B^{(n-1)} \\ C^{(n-1)} \\ D^{(n-1)} \end{pmatrix}. \tag{23}$$

The transfer matrix has the following form:[39]

$$\mathbf{M}^{(n-1,n)} = -\frac{1}{2}\begin{pmatrix} -\alpha\exp[iy_n\Delta] & -\beta\exp[-iy_n\Sigma] & \delta\exp[\Xi] & -\delta\exp[-\Theta] \\ -\beta\exp[iy_n\Sigma] & -\alpha\exp[-iy_n\Delta] & -\delta\exp[\Theta] & \delta\exp[-\Xi] \\ \gamma\exp[iy_nk_y^{(n-1)}] & \gamma\exp[-iy_nk_y^{(n-1)}] & -\eta\exp[k_x\Upsilon] & -\xi\exp[-k_x\Upsilon] \\ \gamma\exp[iy_nk_y^{(n-1)}] & \gamma\exp[-iy_nk_y^{(n-1)}] & -\xi\exp[k_x\Upsilon] & -\eta\exp[-k_x\Upsilon] \end{pmatrix}, \tag{24}$$

where

$$\alpha = \left(1 + \frac{k_y^{(n-1)}\overline{c}_{44}^{(n-1)}}{k_y^{(n)}\overline{c}_{44}^{(n)}}\right), \quad \beta = \left(1 - \frac{k_y^{(n-1)}\overline{c}_{44}^{(n-1)}}{k_y^{(n)}\overline{c}_{44}^{(n)}}\right),$$

$$\gamma = \left(1 - \frac{e_{15}^{(n-1)}\varepsilon_{11}^{(n)}}{e_{15}^{(n)}\varepsilon_{11}^{(n-1)}}\right), \quad \delta = i\frac{k_x(e_{15}^{(n-1)})^2}{k_y^{(n)}\overline{c}_{44}^{(n)}\varepsilon_{11}^{(n-1)}}\left(1 - \frac{e_{15}^{(n)}\varepsilon_{11}^{(n-1)}}{e_{15}^{(n-1)}\varepsilon_{11}^{(n)}}\right),$$

$$\eta = \left(\frac{e_{15}^{(n-1)}\varepsilon_{11}^{(n)}}{e_{15}^{(n)}\varepsilon_{11}^{(n-1)}} + \frac{e_{15}^{(n-1)}}{e_{15}^{(n)}}\right), \quad \xi = \left(\frac{e_{15}^{(n-1)}\varepsilon_{11}^{(n)}}{e_{15}^{(n)}\varepsilon_{11}^{(n-1)}} - \frac{e_{15}^{(n-1)}}{e_{15}^{(n)}}\right),$$

$$\Delta = (k_y^{(n-1)} - k_y^{(n)}), \quad \Sigma = (k_y^{(n)} + k_y^{(n-1)}),$$

$$\Xi = (k_x\Upsilon - iy_nk_y^{(n)}), \quad \Theta = (k_x\Upsilon + iy_nk_y^{(n)}),$$

$$\Upsilon = y_n - y_{n-1}. \tag{25}$$

The first block (2×2) of $\mathbf{M}^{(n-1,n)}$ has the usual form of the transfer matrix describing elastic waves[40–42] but with $\overline{c}_{44}$ instead of c_{44}. Note that $\overline{c}_{44}$ appears explicitly and implicitly through Eq. (14), which gives the value of k_y. For the finite systems the matrix $\mathbf{M}$ of order (4×4) defined as the product

$$\mathbf{M} = \mathbf{M}^{(N-1,N)} \cdot \mathbf{M}^{(N-2,N-1)} \cdots \mathbf{M}^{(n-1,n)} \cdots \mathbf{M}^{(0,1)} \cdot \mathbf{M}^{(-1,0)} \tag{26}$$

relates the coefficients $A^{(-1)}$, $B^{(-1)}$, $C^{(-1)}$, and $D^{(-1)}$ of the left semi-infinite medium $(n=-1)$ with the coefficients $A^{(N)}$, $B^{(N)}$, $C^{(N)}$, and $D^{(N)}$ of the last layer $(n=N)$ by means of

$$\begin{pmatrix} A^{(N)} \\ B^{(N)} \\ C^{(N)} \\ D^{(N)} \end{pmatrix} = \mathbf{M} \begin{pmatrix} A^{(-1)} \\ B^{(-1)} \\ C^{(-1)} \\ D^{(-1)} \end{pmatrix}, \tag{27}$$

which establishes four relations between eight coefficients.

B. BC at $y<y_0$ and $y>y_N$ for finite systems and their implications

For the boundary conditions at the two semi-infinite media ($y<y_0$ and $y>y_N$) we have the following statement. Because we only are interested in bound solutions for all values of y we must take

$$D^{(-1)} = 0, \quad C^{(N)} = 0 \tag{28}$$

where, as before, the coefficients $D^{(-1)}$ and $C^{(N)}$ are defined in Eq. (17) for the cases $n=-1$ and $n=N$, respectively. Finally, the other two conditions come from the normalization of the transmitted wave traveling to the right, i.e., $A^{(N)}=1$

and from the fact that we have no incident waves from the right ($B^{(N)}=0$). Therefore we have four conditions given by Eq. (27) in order to determine the same number of unknown coefficients: $A^{(-1)}$, $B^{(-1)}$, $C^{(-1)}$, and $D^{(N)}$. These coefficients are calculated rearranging Eq. (27) and we obtain

$$\begin{pmatrix} A^{(-1)} \\ B^{(-1)} \\ C^{(-1)} \\ D^{(N)} \end{pmatrix} = \mathbf{B}^{-1}\cdot\mathbf{B}' \begin{pmatrix} A^{(N)} \\ B^{(N)} \\ C^{(N)} \\ D^{(-1)} \end{pmatrix} = \mathbf{B}^{-1}\cdot\mathbf{B}' \begin{pmatrix} 1 \\ 0 \\ 0 \\ 0 \end{pmatrix}, \quad (29)$$

where

$$\mathbf{B} = \mathbf{M}\cdot\mathbf{I}_3 - \mathbf{I} + \mathbf{I}_3 = \begin{pmatrix} m_{11} & m_{12} & m_{13} & 0 \\ m_{21} & m_{22} & m_{23} & 0 \\ m_{31} & m_{32} & m_{33} & 0 \\ m_{41} & m_{42} & m_{43} & -1 \end{pmatrix} \equiv \begin{pmatrix} \mathbf{B}_1 & 0 \\ \mathbf{B}_2 & -1 \end{pmatrix}, \quad (30)$$

$$\mathbf{B}' = \mathbf{M}\cdot(\mathbf{I}_3 - \mathbf{I}) + \mathbf{I}_3 = \begin{pmatrix} 1 & 0 & 0 & -m_{14} \\ 0 & 1 & 0 & -m_{24} \\ 0 & 0 & 1 & -m_{34} \\ 0 & 0 & 0 & -m_{44} \end{pmatrix}, \quad (31)$$

$$\mathbf{I}_3 = \begin{pmatrix} 1 & 0 & 0 & 0 \\ 0 & 1 & 0 & 0 \\ 0 & 0 & 1 & 0 \\ 0 & 0 & 0 & 0 \end{pmatrix}, \quad \mathbf{I} = (\delta_{ij}), \quad i,j = 1,\ldots,4. \quad (32)$$

$\mathbf{B}_1$ and $\mathbf{B}_2$ are matrices of order 3×3 and 1×3, respectively, and m_{ij} is the ij element of the transfer matrix $\mathbf{M}$. The inverse of matrix $\mathbf{B}$ can be found as the inverse of the partitioned matrix defined in Eq. (30) as follows:

$$\mathbf{B}^{-1} = \begin{pmatrix} \mathbf{B}_1^{-1} & 0 \\ \mathbf{B}_2\cdot\mathbf{B}_1^{-1} & -1 \end{pmatrix}. \quad (33)$$

In Sec. V we will discuss the properties of coefficients $A^{(-1)}$, $B^{(-1)}$, $C^{(-1)}$, and $D^{(N)}$ as given by Eq. (29). We recall that the transmission and the reflection coefficients are defined as $T\equiv|A^{(N)}|^2/|A^{(-1)}|^2$ and $R\equiv|B^{(-1)}|^2/|A^{(-1)}|^2$, respectively. These definitions are also used in the NSWA. However, in this case all matrices appearing in Eq. (26) must be taken as matrices of order (2×2) which are the first blocks (2×2) of the matrices $\mathbf{M}^{(n-1,n)}$ given by Eq. (24).

C. Global condition for infinite systems and their implications

For infinite systems we will consider only periodic structures with period p. Now the solutions can be characterized by an irreducible representation (irrep) of the group of translations by a finite amount p. As a matter of fact, since the solutions of Eqs. (7) and (8) are of the form $\phi(x,y,t) = \overline{\phi}(y)\exp[i(k_x x-\omega t)]$ and $u_3(x,y,t)=\overline{u_3}(y)\exp[i(k_x x-\omega t)]$, the system of equations can be rewritten as the following eigenvalue equation:

$$\boldsymbol{O}\mathbf{S}(y) = \lambda\mathbf{S}(y), \quad (34)$$

where $\mathbf{S}(y)=[\overline{\phi}(y),\overline{u_3}(y)]^T$ and $\boldsymbol{O}$ is a matrix differential operator, which is invariant under translations of the form $y\rightarrow y+jp$. In other words, $\boldsymbol{O}$ commutes with the corresponding translation operator τ_{jp}, j being an arbitrary integer. Therefore there exist solutions of Eq. (34) which also are eigenfunctions of τ_{jp}.[43–46] Thus we will look for solutions $\mathbf{S}(y)$ satisfying

$$\tau_{jp}\mathbf{S}(y) = \exp[i\kappa jp]\mathbf{S}(y), \quad (35)$$

where the eigenvalue $\exp[i\kappa jp]$ is the one-dimensional irrep for the element τ_{jp} of the Abelian discrete group of translations and κ is the index of the irrep or Bloch's wave number. If we use the property $\tau_{jp}\mathbf{S}(y)=\mathbf{S}(y+jp)$ in Eq. (35) we obtain the Bloch condition, that for the case $j=1$, becomes

$$\overline{\phi}(y+p) = \exp[i\kappa p]\overline{\phi}(y) \quad (36)$$

and

$$\overline{u_3}(y+p) = \exp[i\kappa p]\overline{u_3}(y). \quad (37)$$

Because these equations are valid for all values of y and the exponential functions are linearly independent we have

$$A^{(n+m)}\exp[ik_y^{(n+m)}(y+p)] = \exp[i\kappa p]A^{(n)}\exp[ik_y^{(n)}y], \quad (38)$$

$$B^{(n+m)}\exp[-ik_y^{(n+m)}(y+p)] = \exp[i\kappa p]B^{(n)}\exp[-ik_y^{(n)}y], \quad (39)$$

$$C^{(n+m)}\exp[k_x(y+p-y_{n+m})] = \exp[i\kappa p]C^{(n)}\exp[k_x(y-y_n)], \quad (40)$$

$$D^{(n+m)}\exp[-k_x(y+p-y_{n+m})] = \exp[i\kappa p]D^{(n)}\exp[-k_x(y-y_n)], \quad (41)$$

where n is an arbitrary integer and m is the number of layers in each period, that is, $p=y_{n+m}-y_n$. Due to the periodicity $k_y^{(n+m)}=k_y^{(n)}$ and Eqs. (38)–(41) can be written as

$$\begin{pmatrix} A^{(n+m)}\exp[ik_y^{(n)}p] \\ B^{(n+m)}\exp[-ik_y^{(n)}p] \\ C^{(n+m)} \\ D^{(n+m)} \end{pmatrix} = \mathbf{E}\begin{pmatrix} A^{(n+m)} \\ B^{(n+m)} \\ C^{(n+m)} \\ D^{(n+m)} \end{pmatrix} = e^{i\kappa p}\begin{pmatrix} A^{(n)} \\ B^{(n)} \\ C^{(n)} \\ D^{(n)} \end{pmatrix}, \quad (42)$$

where

$$\mathbf{E} = \begin{pmatrix} \exp[ik_y^{(n)}p] & 0 & 0 & 0 \\ 0 & \exp[-ik_y^{(n)}p] & 0 & 0 \\ 0 & 0 & 1 & 0 \\ 0 & 0 & 0 & 1 \end{pmatrix}. \quad (43)$$

On the other hand, from the properties of the transfer matrices, there exists other relation between the coefficients of the $(n+m)$-layer with the ones of the n-layer, which reads

$$\begin{pmatrix} A^{(n+m)} \\ B^{(n+m)} \\ C^{(n+m)} \\ D^{(n+m)} \end{pmatrix} = \mathbf{M}_p^{(n)} \begin{pmatrix} A^{(n)} \\ B^{(n)} \\ C^{(n)} \\ D^{(n)} \end{pmatrix}, \tag{44}$$

where

$$\mathbf{M}_p^{(n)} \equiv \mathbf{M}^{(n+m-1,n+m)} \cdot \mathbf{M}^{(n+m-2,n+m-1)} \cdots \mathbf{M}^{(n,n+1)}. \tag{45}$$

Therefore

$$\mathbf{EM}_p^{(n)} \begin{pmatrix} A^{(n)} \\ B^{(n)} \\ C^{(n)} \\ D^{(n)} \end{pmatrix} = \exp[i\kappa p] \begin{pmatrix} A^{(n)} \\ B^{(n)} \\ C^{(n)} \\ D^{(n)} \end{pmatrix}. \tag{46}$$

The dispersion relation k vs $\omega/2\pi$ is given implicitly by

$$\det(\mathbf{EM}_p^{(n)} - \mathbf{I} \exp[i\kappa p]) = 0, \tag{47}$$

where the angle of incidence θ is a constant. However, we will be also interested in a similar relation of the form κ vs $\sin^2\theta$ which is again given implicitly by Eq. (47) but now with the frequency equal to a constant. This relation will be called *angular dispersion relation*.

In order to simplify the calculations we will use the symmetries of the system. We will write the characteristic polynomial in $\Lambda \equiv \exp[i\kappa p]$, $P(\Lambda) = \det(\mathbf{EM}_p^{(n)} - \mathbf{I} \exp[i\kappa p])$, as[47]

$$P(\Lambda) = \Lambda^2(\Lambda^2 + a_3\Lambda + a_2 + a_1/\Lambda + a_0/\Lambda^2), \tag{48}$$

where $a_3 = -\mathrm{Tr}\{\mathbf{EM}_p^{(n)}\}$, $a_2 = [(\mathrm{Tr}\{\mathbf{EM}_p^{(n)}\})^2 - \mathrm{Tr}\{(\mathbf{EM}_p^{(n)})^2\}]/2$, and $a_0 = \det\{\mathbf{EM}_p^{(n)}\}$. The symbol $\mathrm{Tr}\{(\cdot)\}$ means trace of a matrix $\cdot$. Now we remark that if κ is a solution of Eq. (47) representing a Bloch wave traveling towards the right, then $-\kappa$ is also a solution and it represents the same wave but traveling towards the left. Therefore if Λ is a zero of $P(\Lambda)$, so is $1/\Lambda$. From Eq. (48) we see that we should have $a_1 = a_3$ and $a_0 = 1$. Therefore the fourth-order equation in $\exp[i\kappa p]$ can be written as

$$0 = \Lambda^2 + \Lambda^{-2} + a_3[\Lambda + \Lambda^{-1}] + a_2 = 4\cos^2(\kappa p) + 2a_3\cos(\kappa p) + a_2 - 2 \tag{49}$$

from which the four values κ_1, κ_2, κ_3, and κ_4 of κ are calculated. We should mention that not each 4×4 matrix describing layered media has the above-mentioned properties. However, due to the symmetries of our system, matrix $\mathbf{EM}_p^{(n)}$ has those properties. This fact was used to check our numerical calculations.

For each value κ_j there is a solution $\mathbf{X}_j^{(n)}$ to the equation

$$[\mathbf{EM}_p^{(n)} - \mathbf{I} \exp[ip\kappa_j]]\mathbf{X}_j^{(n)} = 0. \tag{50}$$

If the eigenvector $\mathbf{X}_j^{(n)}$ is written as $\mathbf{X}_j^{(n)} = (\boldsymbol{A}_j^{(n)}, \boldsymbol{B}_j^{(n)}, \boldsymbol{C}_j^{(n)}, \boldsymbol{D}_j^{(n)})^T$, where n is the index associated with the nth layer, which is, of course, arbitrary, we have the following four eigensolutions to the nth layer:

$$[\overline{u}_3^{(n)}(y)]_j = \frac{\varepsilon_{11}^{(n)}}{e_{15}^{(n)}}(\boldsymbol{A}_j^{(n)} \exp[ik_y^{(n)}y] + \boldsymbol{B}_j^{(n)} \exp[-ik_y^{(n)}y]), \tag{51}$$

$$\overline{\phi}_j^{(n)}(y) = \boldsymbol{A}_j^{(n)} \exp[ik_y^{(n)}y] + \boldsymbol{B}_j^{(n)} \exp[-ik_y^{(n)}y] + \boldsymbol{C}_j^{(n)} \times \exp[k_x(y-y_n)] + \boldsymbol{D}_j^{(n)} \exp[-k_x(y-y_n)] \tag{52}$$

for $j = 1,2,3,4$.

In the NSWA, where the surface waves are neglected, the dispersion relation κ vs $\omega/2\pi$ and the angular dispersion relation κ vs $\sin^2\theta$ are defined implicitly by

$$\det\{\overline{\mathbf{EM}}_p^{(n)} - \mathbf{I} \exp[i\kappa p]\} = 0, \tag{53}$$

where $\overline{\mathbf{E}}$ is the first blocks of order 2×2 of $\mathbf{E}$ and $\overline{\mathbf{M}}_p^{(n)}$ is given by Eq. (45). However, now all matrices appearing there must be taken as matrices of order (2×2) which are the first blocks (2×2) of the matrices $\mathbf{M}^{(n-1,n)}$ given by Eq. (24). Therefore we only have two values for κ with $\kappa_1 = -\kappa_2$. Furthermore, because of the periodicity $\det\{\overline{\mathbf{EM}}_p^{(n)}\} = 1$ and κ_i can be calculated from

$$\cos(\kappa p) = \frac{1}{2}\mathrm{Tr}\{\overline{\mathbf{EM}}_p^{(n)}\}. \tag{54}$$

The coefficients $\boldsymbol{A}_j^{(n)}$, $\boldsymbol{B}_j^{(n)}$ associated with the two eigensolutions $\overline{\phi}_1^{(n)}(y)$ and $\overline{\phi}_2^{(n)}(y)$ are obtained by solving

$$[\overline{\mathbf{EM}}_p^{(n)} - \mathbf{I} \exp[ip\kappa_j]]\overline{\mathbf{X}}_j^{(n)} = 0, \tag{55}$$

where $\overline{\mathbf{X}}_j^{(n)} = (\boldsymbol{A}_j^{(n)}, \boldsymbol{B}_j^{(n)})^T$ with $j = 1,2$ and

$$\overline{\phi}_j^{(n)}(y) = \frac{e_{15}^{(n)}}{\varepsilon_{11}^{(n)}}[\overline{u}_3^{(n)}(y)]_j = \boldsymbol{A}_j^{(n)} \exp[ik_y^{(n)}y] + \boldsymbol{B}_j^{(n)} \exp[-ik_y^{(n)}y]. \tag{56}$$

V. ANALYSIS OF THE RESULTS

We first consider finite piezocomposites. Figure 3 shows plots T vs f for fixed values of the angle of incidence θ. f is frequency in hertz: $f = \omega/2\pi$. In Fig. 3(a) we consider the system analyzed in Fig. 2 of Ref. 12 where the NSWA was used and only one period was taken into account. The values of the quantities $c_{44}^{(n)}$, $e_{15}^{(n)}$, $\varepsilon_{11}^{(n)}$, and $\rho^{(n)}$ were taken from that reference. Dotted lines correspond to the NSWA and solid lines to the exact calculation where the surface waves are taken into account. In the upper curve the dotted and solid lines coincide. The dotted lines reproduce exactly the curves (1), (2), and (3) of Fig. 2 of Ref. 12 which correspond to angles of incidence $\theta = 0°$, 30° and 60°, respectively. Figure 3(a) shows that the larger the angle of incidence is, the more different are the results of the NSWA and the exact calculation. In fact, the curves corresponding to $\theta = 0$ are the same. This is so because $\theta = 0$ implies $k_x = 0$ and $\delta = 0$. Thus the matrices $\mathbf{M}^{(n-1,n)}$ are of the form [see Eqs. (14), (24), and (25)]

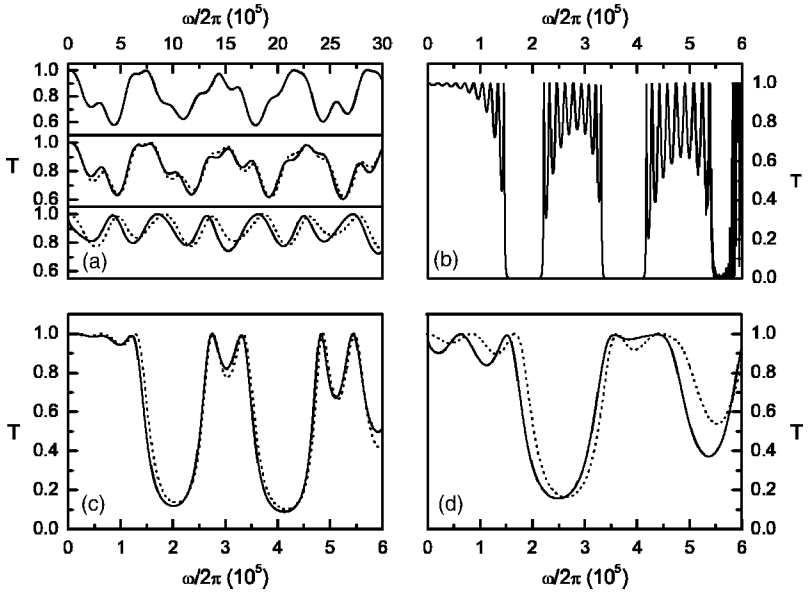

FIG. 3. Transmission coefficient T as a function of frequency $f=\omega/2\pi$ for different fixed values of the angle of incidence θ. In all figures the dotted lines correspond with the NSWA and the solid lines with the exact calculations. In (a) we show three solid lines corresponding with angles of incidence $\theta=0°$ (upper curve), 30°, and 60° (bottom curve), respectively. The structure of the Piezocomposite is ZnO|PZT4|PZT5A|PZT5H|CdS|ZnO, with the same layer width ($d=1.25$ mm), which is the system analyzed in Fig. 2 of Ref. 12. The parameters in (b) are the same as in (a) but now the sequence of layers PZT4|PZT5A|PZT5H|CdS|ZnO is repeated ten times (ten periods), $\theta=10°$ and the interval of frequency is shorter. The parameters in (c) and (d) are the same as in (b), but now we only have three periods. The corresponding values of θ are 30° and 60°, respectively.

$$\begin{pmatrix} \mathbf{M}_{11} & \mathbf{O} \\ \mathbf{M}_{21} & \mathbf{M}_{22} \end{pmatrix}, \tag{57}$$

where $\mathbf{M}_{ij}$ and $\mathbf{O}$ are matrices of order 2×2 and $\mathbf{O}$ is the zero matrix. Furthermore, because the product of two matrices of the form (57) is

$$\begin{pmatrix} \mathbf{A}_{11} & \mathbf{O} \\ \mathbf{A}_{21} & \mathbf{A}_{22} \end{pmatrix}\begin{pmatrix} \mathbf{B}_{11} & \mathbf{O} \\ \mathbf{B}_{21} & \mathbf{B}_{22} \end{pmatrix} = \begin{pmatrix} \mathbf{A}_{11}\mathbf{B}_{11} & \mathbf{O} \\ \mathbf{C} & \mathbf{A}_{22}\mathbf{B}_{22} \end{pmatrix} \tag{58}$$

with $\mathbf{C}=\mathbf{A}_{21}\mathbf{B}_{11}+\mathbf{A}_{22}\mathbf{B}_{21}$, the first 2×2 block of matrix $\mathbf{M}$ of Eq. (26) is equal to the product of the first 2×2 blocks of matrices $\mathbf{M}^{(n-1,n)}$. Therefore for the case $\theta=0°$ the calculations of the transmission and reflection coefficients must be the same for the NSWA and for the exact approach. For other values of θ the second block of $\mathbf{M}^{(n-1,n)}$ is not equal to $\mathbf{O}$ but we can expect that for small values of θ both calculations give very similar results as shown in Fig. 3(a). We have observed that this fact is also true for all the configurations analyzed. In particular for those considered in Ref. 12, even in systems having polymer bonding of araldite at each interface. So, the calculations of the transmission and reflection coefficients for small angles can be done approximately by using the NSWA, which is easier, numerically stable, and faster.

Figure 3(b) also shows a plot T vs $\omega/2\pi$ but now for a system with ten periods, $\theta=10°$ and $\omega/2\pi\in[0,6\times 10^5]$. The values of the other parameters are as in Fig. 3(a). We have increased the number of periods from 1 to 10 in order to have well shaped bands. In fact, in this figure we clearly see a band structure for the transmission coefficient with three gaps and four bands (one of them incomplete) in the analyzed interval of frequency. A detailed observation of the curve shows that each complete band has nine maxima as it must be. In fact, because the system has ten periods, it has nine cells each of them able to catch a resonance. In this case the curve corresponding to the NSWA is not shown for clarity but it will be considered below. In this figure the system has $10\times 5=50$ layers and the calculations become unstable for large values of frequencies, angle of incidence, and width of the layers. This fact causes the broadening of the curve at the right side of the plot. For this reason, in Figs. 3(c) and 3(d), we have taken only three periods. Now the curves have less structure and one can clearly see the differences between the NSWA (dotted lines) and the exact calculation (solid lines). In Fig. 3(c) the value of θ is smaller than that in Fig. 3(d), therefore the two curves of Fig. 3(c) are more similar to each other than the two curves of Fig. 3(d). Figure 3 also shows that the larger the number of periods is, the better is the shape of the bands. So, if we want to have a well-defined profile for the bands we need to have a larger number of layers.

For nonperiodic systems the band structure is, of course, broken, but for small angles of incidence the NSWA is still a good approximation. See, for example, the plots T vs $\omega/2\pi$ shown in Fig. 4. This figure corresponds to a multilayered system built according to the Fibonacci sequence $\mathbf{S}_9$, such that the nth sequence $\mathbf{S}_n$ is equal to the juxtapositions of the $(n-1)$th sequence $\mathbf{S}_{n-1}$ with the $(n-2)$th sequence $\mathbf{S}_{n-2}$, that is,

$$\mathbf{S}_n = \mathbf{S}_{n-1}\mathbf{S}_{n-2}, \tag{59}$$

where $\mathbf{S}_1=A$, $\mathbf{S}_2=AB$, and the bocks A, B are defined in the caption of the figure. This sequence is an example of quasiperiodic structures which, in the last years, have received much attention because of their intermediate properties between periodic and disordered systems. In particular, these kinds of systems have been used to study the evolution of the band structure when the degree of disorder of the system changes from perfectly ordered to a Fibonacci sequence (see, for example, Ref. 48). In Fig. 4 the number of layers is equal to 55 which, for a periodic system, is sufficient to have well-shaped bands. However, Fig. 4 shows that for this Fibonacci sequence we do not have well-defined bands neither in NSWA nor in exact calculation.

Some interesting properties of layered piezocomposites can be also studied if one analyzes the transport properties as

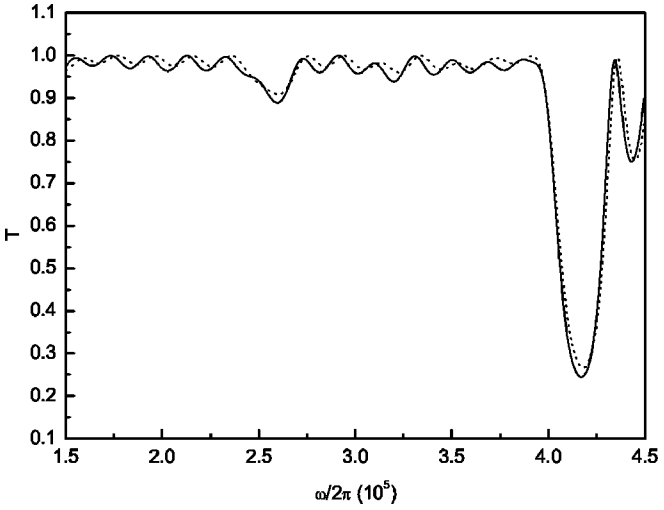

FIG. 4. Plots of T as a function of frequency f for a fixed value of the angle of incidence $\theta=30°$. The structure of the piezocomposite is a Fibonacci sequence with two blocks A, B of the type A =PZT4 and B=PZT5A with the same layer width (d=1.25 mm). The system is embedded between two layers of ZnO.

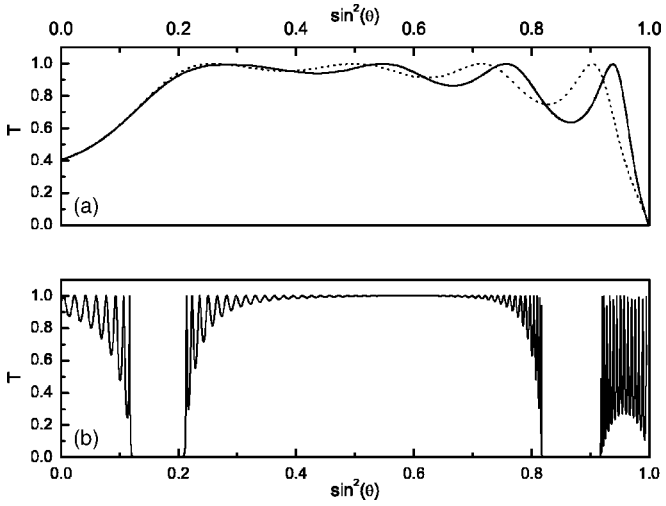

FIG. 5. Plots of T as a function of $\sin^2\theta$ for a fixed value of frequency. In (a) $f=1.2\times10^6$ and the piezocomposite is a sequence of ten periods where each period is formed with two blocks (the blocks A, B considered in Fig. 4). The system is embedded between two layers of ZnO. In (b) $f=(2/\pi)\times10^7$ and we have taken 49 periods. Now the blocks A, B are as in Fig. 4 of Ref. 39 and they have the following parameters: $p^{(0)}=p_A=5.\times10^{-5}$ m, $p^{(-1)}=p_B=15.\times10^{-5}$ m, $\rho^{(n)}=\rho_A=\rho_B=2500$ kg/m^3, $\varepsilon_{11}^{(0)}=\varepsilon_{11}^{A}=44.43\times10^{-10}$ F/m, $\varepsilon_{11}^{(-1)}=\varepsilon_{11}^{B}=64.63\times10^{-10}$ F/m, $e_{15}^{(0)}=e_{15}^{A}=0.6875$ C/m^2, $e_{15}^{(-1)}=e_{15}^{B}=1$ C/m^2, $c_{44}^{(0)}=c_{44}^{A}=1/4\times10^{10}$ N/m^2, and $c_{44}^{(-1)}=c_{44}^{B}=4/11\times10^{10}$ N/m^2. In this case the dotted and solid lines coincide because the parameters obey relations of the form given by Eqs. (60)–(63) and therefore the matrices are as in expression (64) (see Ref. 39 for details).

a function of the angle of incidence. In these cases the left side of the curves (that is, $0\leqslant\theta\ll90°$) for the NSWA and for the exact calculation must coincide, but, in general, they must become different for large values of θ. For example, in Fig. 5(a) we have two plots T vs $\sin^2\theta$ for a sequence of ten periods with two different blocks in each period. We see that the dotted and solid lines coincide for small values of θ. If we increase the number of periods we obtain a well-defined band structure similar to the band structure of the plots T vs $\omega/2\pi$ shown in previous figures. In Fig. 5(b) we show a plot of this type for a system with 49 periods. A detailed analysis of the results shows that the plot has 48 peaks in the complete central band. However, in this case, we have considered a different periodic structure as in Fig. 5(a). Now the dotted and solid lines coincide for all values of θ. This is so because the system is of a special kind as the one considered in Ref. 39. In this system the material constants obey the linear relations

$$e_{15}^{(n)}=\Omega c_{44}^{(n)}, \tag{60}$$

$$e_{15}^{(n)}=\Gamma\varepsilon_{11}^{(n)}, \tag{61}$$

$$\varepsilon_{11}^{(n)}/c_{44}^{(n)}=\Omega/\Gamma, \tag{62}$$

$$\rho^{(n+1)}=\rho^{(n)} \quad \forall\ n,m, \tag{63}$$

where Ω, Γ are two constants independent of the script (n). Therefore $\bar{c}_{44}^{(n)}=c_{44}^{(n)}(1+\Omega\Gamma)$. In this case the matrix $\mathbf{M}^{(n-1,n)}$ reduces to [see Eqs. (24) and (25)]

$$\begin{pmatrix}\mathbf{M}_{11} & \mathbf{O}\\ \mathbf{O} & \mathbf{M}_{22}\end{pmatrix}, \tag{64}$$

for all values of θ. Therefore all the comments following Eq. (57) are applicable and the exact calculations give the same results as the ones of the NSWA.

As for the plots T vs $\omega/2\pi$, if the periodicity of the systems is broken, the band structure of the plots T vs θ is destroyed. An interesting example of this is when the values of the piezoelectric parameters of the layers obey a linear variation of the form [see Fig. 6(a)]

$$\left(\frac{\rho\omega^2}{\bar{c}_{44}}\right)^{(j\pm2m)}=\left(\frac{\rho\omega^2}{\bar{c}_{44}}\right)^{(j)}\pm mpF, \tag{65}$$

where F is an arbitrary constant, m and j arbitrary integers, $p=p_1+p_2$, and $(\rho\omega^2/\bar{c}_{44})^{(j)}$ represents the values of the magnitude $\rho\omega^2/\bar{c}_{44}$ at the jth layer, that is, $(\rho\omega^2/\bar{c}_{44})^{(j)}\equiv\rho^{(j)}\omega^2/\bar{c}_{44}^{(j)}=(\rho\omega^2/\bar{c}_{44})(y)$ for $y\in[y_j,y_{j+1}]$. Now the system is nonperiodic and it has been shown[39,49,50] that the plots T vs $\sin^2\theta$ must show a sequence of peaks (resonances) separated a distance Δ proportional to the slope of the dotted line shown in Fig. 6(a). These peaks are called Stark-Ladder resonances (SLR). Figure 6(b) shows a plot of this kind where we have used piezoelectric parameters that obey Eq. (69). This figure shows clearly that the band structure has disappeared, and a Stark-Ladder structure appears instead. This property is analogous to the one observed in the electronic spectrum of crystals in the presence of uniform electric fields. The SLR were predicted in 1961 by Wannier,[51] and observed experimentally in 1989 by Mendez *et al.*[52] The physics behind the SLR is a phenomenon of alternating constructive and destructive interference as in a Fresnel

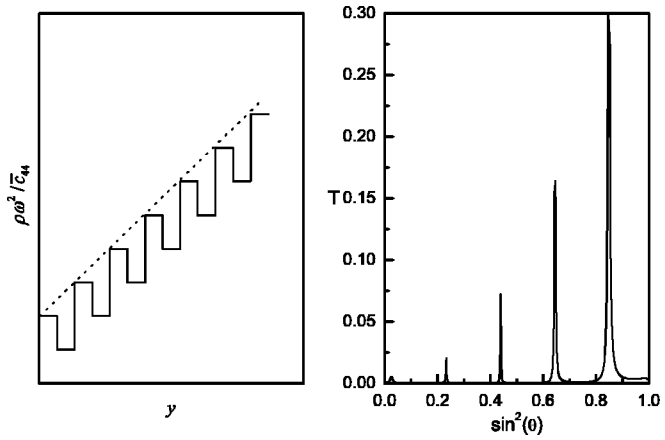

FIG. 6. (a) Plot of $\rho\omega^2/\overline{c_{44}}$ as a function of the coordinate y (in arbitrary units) when $\rho\omega^2/\overline{c_{44}}$ satisfies Eq. (65). The slope of the dashed line is equal to F. For the periodic case $F=0$. (b) Transmission coefficient as a function of $\sin^2\theta$ for a composite with parameters satisfying a relation of the form plotted in (a). The plot shows the SLR. The parameters are as in Fig. 5(b) except $\varepsilon_{11}^{(0)}=10.6825\times10^{-10}$ F/m, $e_{15}^{(0)}=0.6875$ C/m^2, $c_{44}^{(0)}=(80/121)\times10^{10}$ N/m^2, $c_{44}^{(-1)}=4\times10^{10}$ N/m^2. The values of the parameters for other values of n are obtained from Eq. (65) with $F=9961.64$ m^{-3}. However, the parameters still obey relations of the form given by Eqs. (60)–(63) and therefore the dotted and solid lines coincide.

interferometer.[39,49,50] Since in this example we have used also Eqs. (60)–(63) the curves are unchanged when one neglects the surface waves. However, for other analyses they are necessary as we will see below.

Now we consider an infinite number of periods. From Eq. (47) we obtain four dispersion relations κ_j vs $\omega/2\pi$. However, as discussed, $\kappa_1=-\kappa_2$ and $\kappa_3=-\kappa_4$. Therefore we will analyze only the dispersion relations for κ_1 and κ_3. For the NSWA we have only two dispersion relations κ_j vs $\omega/2\pi$, with $\kappa_1=-\kappa_2$ and therefore we will analyze only the dispersion relation for κ_1.

Figure 7 shows plots of Re$\{p\kappa_1\}$, Im$\{p\kappa_1\}$, Re$\{p\kappa_3\}$, and Im$\{p\kappa_3\}$ as a function of $\omega/2\pi$ (dispersion curves) for a fixed value of the angle θ. The values of the piezoelectric parameters are as in Fig. 3(b) except that now we have an infinite number of periods. First we will analyze the behavior of κ_1. We note that in the intervals of frequency where the function $\kappa_1=\kappa_1(\omega)$ is imaginary the expression $|\exp[ip\kappa_1]|$ is different from 1 and Block's theorem is not satisfied. Therefore the functions $\overline{\phi_1}$ and $(\overline{u_3})_1$ are not valid solutions for these values of frequency. As a matter of fact, from a comparison between Fig. 3(b) and Figs. 7(a) and 7(c) we observe that Im$\{p\kappa_1\}=0$ in the bands and Im$\{p\kappa_1\}\neq0$ in the gaps. Furthermore, $0<\mathrm{Re}\{p\kappa_1\}<\pi$ in the bands and Re$\{p\kappa_1\}=m\pi$ in the gaps, where $m=0$ or $m=1$. We have observed these characteristics, both for the exact and for the NSWA calculations. However, κ_3 does not show this behavior as will be discussed below. Furthermore, κ_3 does not exist in the NSWA and therefore it must be associated with the behavior of the surface waves.

At this point we must comment on the following: for each value of frequency we obtain, from Eq. (47), four values of κ for the exact calculations and, from Eq. (53), two values for the NSWA. So, when we plot the real and imaginary parts of these four (two) values of κ as a function of frequency ω we obtain eight (four) families of points and we have observed that each family can be joined by means of a continuous line. Furthermore, these results confirm that if κ is a solution to Eq. (47) then $-\kappa$ is also a solution. The decision about which κ is to be root 1 or 2, etc., is, of course, arbitrary but since the curves are continuous one can follow the evolution of each root. However, in some intervals of frequency, where two or more roots have the same value, it is difficult to decide which κ is to be root 1 or 2, etc. In these cases we have used the criterion that the curves for κ_1 and κ_2 for the exact calculations must be similar to those of the NSWA calculations. Note that in the NSWA case we only have two values for κ, and therefore the decision is easy. However, in some other few intervals (where κ_1 and κ_2 for the NSWA

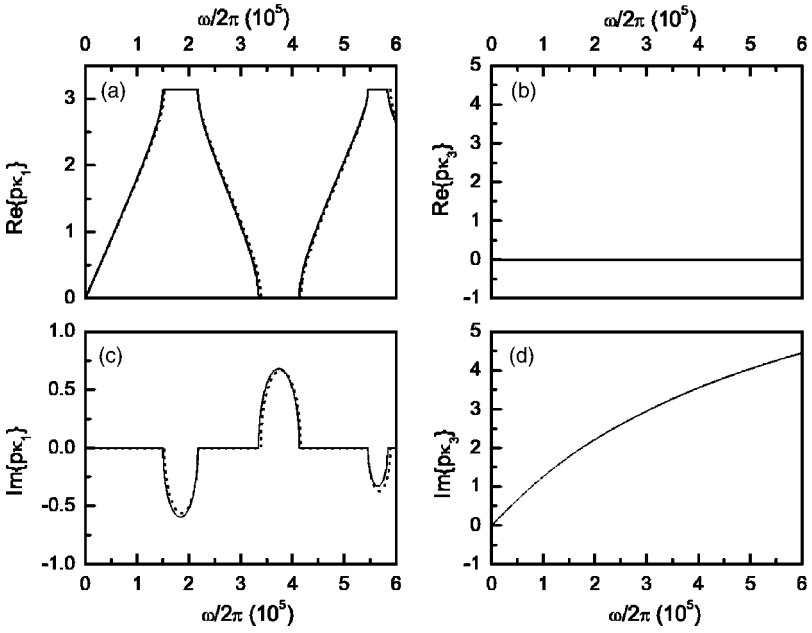

FIG. 7. Dispersion relations κ vs $\omega/2\pi$ for an infinite piezocomposite with parameters as in Fig. 3(b). In (a) and (c) we have the real and imaginary parts of κ_1, respectively, and in (b) and (d) the real and imaginary parts of κ_3, respectively. The figures show four solid lines but only two dotted lines because in the NSWA κ_3 does not exist. The intervals where the solid lines of Re$\{p\kappa_1\}$ are equal to zero or π are [150 412.5, 217 550.9], [335 043.1, 413 571.05], and [546 049.5, 584 414.3].

coincide) our assignation was arbitrary. Therefore our classification of the four curves κ vs $\omega/2\pi$ could be different (in some few intervals) from the classification of the curves of other authors.

The eigenmode associated with κ_1 is obtained from Eq. (50) with $j=1$ [or from Eq. (55) in the NSWA]. Because this equation represents a homogeneous system with four (or two) equations we can assign an arbitrary value to one of the coefficients $\boldsymbol{A}_1^{(n)}, \boldsymbol{B}_1^{(n)}, \boldsymbol{C}_1^{(n)}, \boldsymbol{D}_1^{(n)}$ (or $\boldsymbol{A}_1^{(n)}, \boldsymbol{B}_1^{(n)}$). This offers a lot of possibilities with respect to the relations between the coefficients associated with the exact calculations and those associated with the NSWA. For example, we can assign the same value to the coefficients $\boldsymbol{A}_1^{(n)}$ corresponding with the exact and the NSWA calculations. Another possibility is to assign a fixed value to $\boldsymbol{D}_1^{(n)}=1$ (which is not present in the NSWA) and obtain the other three coefficients from Eq. (50). Then, we can take the above calculated value of $\boldsymbol{A}_1^{(n)}$ to be equal to the corresponding NSWA coefficient $\boldsymbol{A}_1^{(n)}$. However, we can also take two completely different values for these coefficients $\boldsymbol{A}_1^{(n)}$ in both approaches, etc. So, a direct comparison between the coefficients associated with the exact and NSWA calculations has no sense. Therefore in the next two figures we do not include the corresponding NSWA curves. In any case we have observed that the behavior of the eigenmodes reflect the fact that the solutions are extended in the permitted bands of frequency and they are nonphysical in the gaps as we will see below.

Because $\kappa_1=-\kappa_2$ we have $(\exp[ip\kappa_1])^*=\exp[ip\kappa_2]$ in the bands and $(\exp[ip\kappa_1])^*=\exp[ip\kappa_1]$ in the gaps. Therefore $[\overline{\phi}_1^{(n)}(y)]^*$ is proportional to $\overline{\phi}_2^{(n)}(y)$ in the bands and proportional to $\overline{\phi}_1^{(n)}(y)$ in the gaps. Thus if we take $\boldsymbol{D}_1^{(n)}=\boldsymbol{D}_2^{(n)}=1$ we have

$$\boldsymbol{A}_2^{(n)}=\boldsymbol{B}_1^{(n)*}, \quad \boldsymbol{B}_2^{(n)}=\boldsymbol{A}_1^{(n)*}, \quad \boldsymbol{C}_2^{(n)}=\boldsymbol{C}_1^{(n)*} \tag{66}$$

in the bands and

$$\boldsymbol{B}_1^{(n)}=\boldsymbol{A}_1^{(n)*}, \quad \boldsymbol{B}_2^{(n)}=\boldsymbol{A}_2^{(n)*}, \quad \boldsymbol{C}_1^{(n)}=\boldsymbol{C}_1^{(n)*} \tag{67}$$

in the gaps. In Fig. 8 we have plotted some of these coefficients as a function of $\omega/2\pi$. Figures 8(a), 8(c), and 8(e) show plots of $\mathrm{Re}\{\boldsymbol{A}_1^{(0)}\}$, $\mathrm{Re}\{\boldsymbol{B}_1^{(0)}\}$, and $\mathrm{Re}\{\boldsymbol{C}_1^{(0)}\}$ for $\boldsymbol{D}_1^{(0)}=1$ and Figs. 8(b), 8(d), and 8(f) show plots of $\mathrm{Re}\{\boldsymbol{A}_2^{(0)}\}$, $\mathrm{Re}\{\boldsymbol{B}_2^{(0)}\}$, and $\mathrm{Re}\{\boldsymbol{C}_2^{(0)}\}$ for $\boldsymbol{D}_2^{(0)}=1$, for the same system as in Figs. 3(b) and 7. The imaginary part of these coefficients is not shown but it has a very similar behavior as the real part. The same is true for the behavior of the coefficients $\boldsymbol{A}_1^{(n)}$, $\boldsymbol{B}_1^{(n)}$, and $\boldsymbol{C}_1^{(n)}$ for other values of n. From a comparison between Fig. 7(a) [or Fig. 3(b)] with the plots of Fig. 8 we observe that all the coefficients are finite in the bands but some of them diverge in the gaps. Therefore the mathematical expression for the eigenmodes at the 0th layer associated with κ_1 and κ_2,

$$[\overline{u}_3^{(0)}(y)]_1=\frac{\varepsilon_{11}^{(0)}}{e_{15}^{(0)}}(\boldsymbol{A}_1^{(0)}\exp[ik_y^{(0)}y]+\boldsymbol{B}_1^{(0)}\exp[-ik_y^{(0)}y]), \tag{68}$$

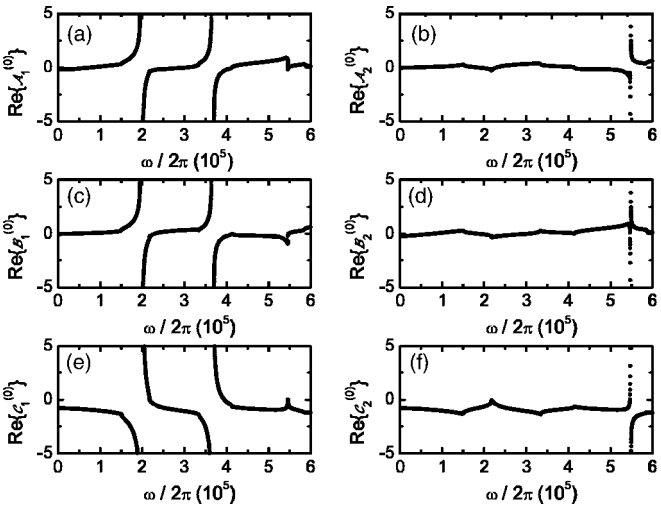

FIG. 8. Plots of the coefficients as a function of $\omega/2\pi$. (a), (c), and (e) are plots of $\mathrm{Re}\{\boldsymbol{A}_1^{(0)}\}$, $\mathrm{Re}\{\boldsymbol{B}_1^{(0)}\}$, and $\mathrm{Re}\{\boldsymbol{C}_1^{(0)}\}$, respectively, with $\boldsymbol{D}_1^{(0)}=1$. (b), (d), and (f) are plots of $\mathrm{Re}\{\boldsymbol{A}_2^{(0)}\}$, $\mathrm{Re}\{\boldsymbol{B}_2^{(0)}\}$, and $\mathrm{Re}\{\boldsymbol{C}_2^{(0)}\}$, respectively, with $\boldsymbol{D}_2^{(0)}=1$. The parameters of the piezocomposite are as in Figs. 3(b) and 7.

$$\overline{\phi}_1^{(0)}(y)=\boldsymbol{A}_1^{(0)}\exp[ik_y^{(0)}y]+\boldsymbol{B}_1^{(0)}\exp[-ik_y^{(0)}y]+\boldsymbol{C}_1^{(0)}\exp[k_xy]+\exp[-k_xy], \tag{69}$$

and

$$[\overline{u}_3^{(0)}(y)]_2=\frac{\varepsilon_{11}^{(0)}}{e_{15}^{(0)}}(\boldsymbol{A}_2^{(0)}\exp[ik_y^{(0)}y]+\boldsymbol{B}_2^{(0)}\exp[-ik_y^{(0)}y]), \tag{70}$$

$$\overline{\phi}_2^{(0)}(y)=\boldsymbol{A}_2^{(0)}\exp[ik_y^{(0)}y]+\boldsymbol{B}_2^{(0)}\exp[-ik_y^{(0)}y]+\boldsymbol{C}_2^{(0)}\exp[k_xy]+\exp[-k_xy], \tag{71}$$

are finite in the bands and diverge in the gaps.

Now we will discuss the properties of κ_3. Figures 7(b) and 7(d) show that the behavior of κ_3 is quite different from those of κ_1 and κ_2. We see that $\mathrm{Re}\{p\kappa_3\}=0$ for all values of frequency. Therefore $\lambda_3=\exp[ip\kappa_3]$ is always a real quantity. Furthermore, as mentioned, because κ_3 and κ_4 do not exist in the NSWA they are associated with the surface waves. This can be also seen from the following reasoning: first we consider an angle of incidence θ equal to zero. Then $k_x=0$ and, due to the periodicity, the product $\mathbf{E}\mathbf{M}_p^{(n)}$ of the matrices $\mathbf{E}$ of Eq. (43) and the transfer matrix $\mathbf{M}_p^{(n)}$ of Eq. (45) reduce to a matrix of the form

$$\begin{pmatrix}\mathbf{M}_{11} & \mathbf{O}\\ \mathbf{M}_{21} & \mathbf{I}\end{pmatrix}, \tag{72}$$

where $\mathbf{M}_{ij}$, $\mathbf{O}$, $\mathbf{I}$ are matrices of order 2×2. $\mathbf{O}$ and $\mathbf{I}$ are the zero and unit matrices, respectively. Furthermore, a plot κ_3 vs $\omega/2\pi$ for the case $\theta=0$ (not shown in a figure) shows that $\kappa_3=0\ \forall\omega$. Thus $\lambda_3=\exp[ip\kappa_3]=1$ and, if we define $\mathbf{a}_3^{(n)}\equiv(\boldsymbol{A}_3^{(n)},\boldsymbol{B}_3^{(n)})^T$ and $\mathbf{c}_3^{(n)}\equiv(\boldsymbol{C}_3^{(n)},\boldsymbol{D}_3^{(n)})^T$, Eq. (50) can be written as

$$\begin{pmatrix} \mathbf{M}_{11} & \mathbf{O} \\ \mathbf{M}_{21} & \mathbf{I} \end{pmatrix} \begin{pmatrix} \mathbf{a}_3^{(n)} \\ \mathbf{c}_3^{(n)} \end{pmatrix} = \begin{pmatrix} \mathbf{M}_{11}\mathbf{a}_3^{(n)} \\ \mathbf{M}_{21}\mathbf{a}_3^{(n)} + \mathbf{c}_3^{(n)} \end{pmatrix} = \lambda_3 \begin{pmatrix} \mathbf{a}_3^{(n)} \\ \mathbf{c}_3^{(n)} \end{pmatrix} = \begin{pmatrix} \mathbf{a}_3^{(n)} \\ \mathbf{c}_3^{(n)} \end{pmatrix}, \tag{73}$$

which implies

$$\mathbf{M}_{11}\mathbf{a}_3^{(n)} = \mathbf{a}_3^{(n)},$$

$$\mathbf{M}_{21}\mathbf{a}_3^{(n)} = \mathbf{O}. \tag{74}$$

These two equations can be satisfied when $\mathbf{a}_3^{(n)} = (0,0)^T$ or when $\mathbf{a}_3^{(n)}$ is an eigenvector of $\mathbf{M}_{11}$ and $\mathbf{M}_{21}$ simultaneously with eigenvalues $\lambda_3 = 1$ and 0, respectively. However, we can see that the only two eigenvalues of the 2×2 matrix $\mathbf{M}_{11}$ are $\lambda_1 = \exp[ip\kappa_1]$ and $\lambda_2 = \exp[ip\kappa_2]$. In fact, from Eq. (50) for $k_x = 0$ and $j = 1,2$ we have

$$\begin{pmatrix} \mathbf{M}_{11} & \mathbf{O} \\ \mathbf{M}_{21} & \mathbf{I} \end{pmatrix} \begin{pmatrix} \mathbf{a}_j^{(n)} \\ \mathbf{c}_j^{(n)} \end{pmatrix} = \lambda_j \begin{pmatrix} \mathbf{a}_j^{(n)} \\ \mathbf{c}_j^{(n)} \end{pmatrix} \quad \Rightarrow \quad \mathbf{M}_{11}\mathbf{a}_j^{(n)} = \lambda_j \mathbf{a}_j^{(n)}. \tag{75}$$

So, the solution to Eqs. (74) is $\mathbf{a}_3^{(n)} = (0,0)^T$ and the eigenvector of the matrix

$$\mathbf{EM}_p^{(n)} = \begin{pmatrix} \mathbf{M}_{11} & \mathbf{O} \\ \mathbf{M}_{21} & \mathbf{I} \end{pmatrix} \tag{76}$$

with eigenvalue $\lambda_3 = 1$ is of the form $(0,0,\boldsymbol{C}_3^{(n)}, \boldsymbol{D}_3^{(n)})^T$. This property was used to check our numerical calculations. That is, we have verified that $\boldsymbol{A}_j^{(n)} = \boldsymbol{B}_j^{(n)} = 0\ \forall\omega$ when $k_x = 0$, $\lambda = 1$, and $j = 3,4$. Therefore κ_3 and κ_4 are associated with the surface waves and they are described by

$$\overline{\phi}_3^{(n)}(y) = \boldsymbol{C}_3^{(n)} \exp[k_x y] + \boldsymbol{D}_3^{(n)} \exp[-k_x y] \tag{77}$$

and

$$\overline{\phi}_4^{(n)}(y) = \boldsymbol{C}_4^{(n)} \exp[k_x y] + \boldsymbol{D}_4^{(n)} \exp[-k_x y] \tag{78}$$

with

$$[\overline{u}_3^{(0)}(y)]_j = 0, \quad j = 3,4. \tag{79}$$

Furthermore, from Eqs. (44), (46), and (73)

$$\begin{pmatrix} \boldsymbol{C}_j^{(n+m)} \\ \boldsymbol{D}_j^{(n+m)} \end{pmatrix} = \begin{pmatrix} \pm\boldsymbol{C}_j^{(n)} \\ \pm\boldsymbol{D}_j^{(n)} \end{pmatrix}, \tag{80}$$

where m is the number of layers in each period, n an arbitrary integer, and $j = 1,2$. Equation (80) implies that the structure of the surface waves repeat periodically with period p.

For the case $k_x \neq 0$ the coefficients $\boldsymbol{A}_3^{(n)}$, $\boldsymbol{B}_3^{(n)}$, $\boldsymbol{A}_4^{(n)}$, and $\boldsymbol{B}_4^{(n)}$ are not equal to zero but they are small as compared with $\boldsymbol{C}_j^{(n)}$ and $\boldsymbol{D}_j^{(n)}$. For example, for the systems considered in Figs. 3(b), 7, and 8, where $\theta = 10°$, the plots of $\boldsymbol{A}_3^{(0)}$, $\boldsymbol{B}_3^{(0)}$, and $\boldsymbol{C}_3^{(0)}$ with $\boldsymbol{D}_3^{(0)} = 1$ are as shown in Fig. 9. In this case the eigenfunction $\overline{\phi}_3(y)$ diverges and is not a physical solution. Furthermore, κ_3 is different from zero but purely imaginary as can be see in Figs. 7(b) and 7(d). Therefore λ_3 is real and $\boldsymbol{B}_3^{(n)} = (\boldsymbol{A}_3^{(n)})^*\ \forall\omega$, as shown in Figs. 9(a)–9(d).

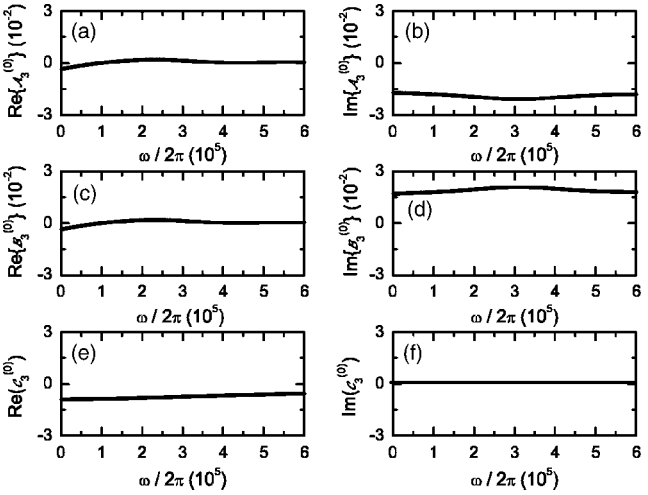

FIG. 9. (a)–(f) Plots of $\mathrm{Re}\{\boldsymbol{A}_3^{(0)}\}$, $\mathrm{Im}\{\boldsymbol{A}_3^{(0)}\}$, $\mathrm{Re}\{\boldsymbol{B}_3^{(0)}\}$, $\mathrm{Im}\{\boldsymbol{B}_3^{(0)}\}$, $\mathrm{Re}\{\boldsymbol{C}_3^{(0)}\}$, and $\mathrm{Im}\{\boldsymbol{C}_3^{(0)}\}$, respectively, as a function of $\omega/2\pi$ with $\boldsymbol{D}_3^{(0)} = 1$. The parameters of the piezocomposite are as in Figs. 3(b), 7, and 8.

Finally we discuss the angular dispersion relation. Figure 10 shows plots of $\mathrm{Re}\{p\kappa_1\}$, $\mathrm{Im}\{p\kappa_1\}$, $\mathrm{Re}\{p\kappa_3\}$, and $\mathrm{Im}\{p\kappa_3\}$ as a function of $\sin^2\theta$ (angular dispersion curves) for a fixed value of the frequency ω. The values of the piezoelectric parameters are as in Fig. 5(b) except that now we have an infinite number of periods. As in Fig. 7, the functions $\overline{\phi}_1$ and $(\overline{u}_3)_1$ are not valid solutions in the intervals of θ where $\kappa_1 = \kappa_1(\sin^2\theta)$ is imaginary. From a comparison between Figs. 5(b) and 10, we observe that $\mathrm{Im}\{p\kappa_1\} = 0$ in the bands and $\mathrm{Im}\{p\kappa_1\} \neq 0$ in the gaps. Furthermore, $0 < \mathrm{Re}\{p\kappa_1\} < \pi$ in the bands and $\mathrm{Re}\{p\kappa_1\} = m\pi$ in the gaps, where $m = 0$ or $m = 1$. The quantity $\mathrm{Re}\{p\kappa_3\}$ is always equal to 0. Indeed, all comments made for Fig. 7 related with the problem of the assignation of the roots, and other properties, are also applicable in Fig. 10, except that now the NSWA and the exact calculations give the same results because the matrices are of the form (64). Furthermore, in this case, a plot $\log(\mathrm{Im}\{p\kappa_3\})$ vs $\log(\sin^2\theta)$ shows that there exists a linear relation between these variables, that is,

$$\log(\mathrm{Im}\{p\kappa_3\}) = C\log(\sin^2\theta) \tag{81}$$

where C is a constant. Therefore

$$\mathrm{Im}\{p\kappa_3\}) = \sin^{2C}\theta. \tag{82}$$

However, for the dispersion curve of Fig. 7(d) we do not have a linear relation between $\log(\mathrm{Im}\{p\kappa_3\})$ and $\log(\omega)$.

VI. CONCLUSIONS

In this work we have analyzed the transport properties of SH and surface waves in heterogeneous finite and infinite piezoelectric media. For "periodic" piezocomposites we have obtained band structures according to the Bloch theorem, both when the response of the systems is studied as a function of frequency and when the response is studied as a function of the angle of incidence. Furthermore, we have corre-

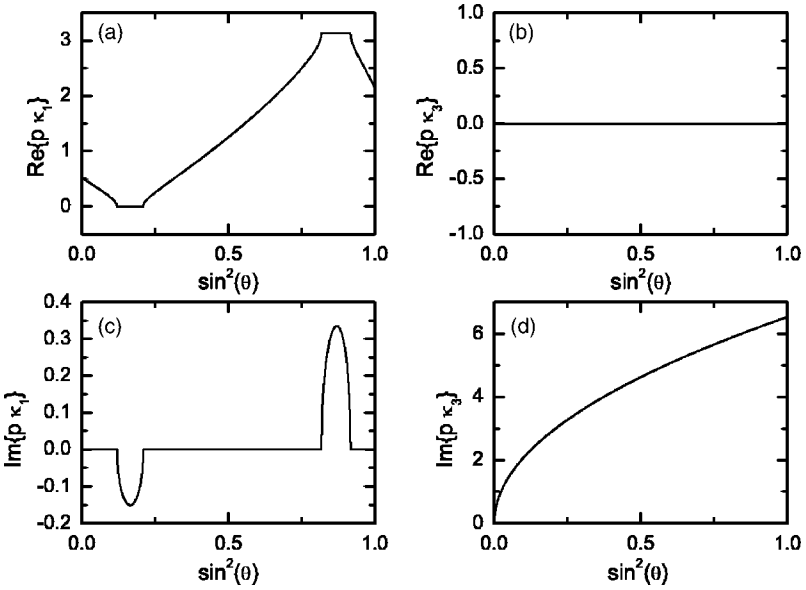

FIG. 10. Angular dispersion relations κ vs $\sin^2\theta$ for an infinite piezocomposite with parameters as in Fig. 5(b). In Figs. 8(a) and 8(c) we have the real and imaginary parts of κ_1, respectively, and in Figs. 8(b) and 8(d) the real and imaginary parts of κ_3, respectively. The figures shows four solid lines but only two dotted lines because in the NSWA κ_3 does not exist. However, the dotted and solid lines coincide because the parameters obey relations of the form given by Eqs. (60)–(63).

lated the structure of the transmission coefficient with the structure of the curves for the dispersion relation and for the angular dispersion relation. For finite systems we have also analyzed the transport properties for some special nonperiodic systems. In particular, in one of them we have obtained Stark-Ladder resonances.

We have also analyzed how the surface waves modify the results obtained from the NSWA. We have considered examples in which these waves can be neglected and others in which these waves affect the NSWA results, including the case when a polymer bonding layer of araldite is placed between each couple of piezoelectric layers. We have seen that this knowledge is important because the fundamental equations describing the piezoelectric effects are a complicated system of equations whose solution is time-consuming and numerically unstable. This is due to the coupling between the mechanical displacements and the electric potential which is described by exponential functions of real argument. So, alternative methods are useful as those mentioned in the text and, in particular, the NSWA.

[1] R. de L. Kronig and W. G. Penney, Proc. R. Soc. London, Ser. A **130**, 499 (1930).
[2] B. Djafari-Rouhani, L. Dobrzynski, O. Hardouin Dupare, R. E. Camley, and A. A. Maradudin, Phys. Rev. B **28**, 1711 (1983).
[3] A. Nougaoui and B. Djafari-Rouhani, Surf. Sci. **185**, 125 (1987); **185**, 154 (1987).
[4] S. Tamura and J. P. Wolfe, Phys. Rev. B **35**, 2528 (1987).
[5] E. H. El Boudouti, B. Djafari-Rouhani, and A. Nougaoui, Phys. Rev. B **51**, 13 801 (1995).
[6] E. L. Shenderov, J. Acoust. Soc. Am. **101**, 1239 (1997).
[7] L. Fernandez, V. R. Velasco, and F. Garcia-Moliner, Surf. Sci. **188**, 140 (1987).
[8] L. P. Zinchuk, A. N. Podlipinets, and N. A. Schul'ga, Sov. Appl. Mech. **24**, 245 (1988).
[9] Li Xingjiao, Li Yibing, Li Shaoping, L. E. Cross, and R. E. Newnham, J. Phys.: Condens. Matter **2**, 9577 (1990).
[10] V. I. Alshits and A. L. Shuvalov, Phys. Lett. A **177**, 253 (1993); , J. Appl. Phys. **77**, 2659 (1995).
[11] V. I. Alshits, A. S. Gorkunova, and A. L. Shuvalov, J. Exp. Theor. Phys. **83**, 509 (1996).
[12] A. A. Alvarez-Mesquida, R. Rodriguez-Ramos, F. Comas, G. Monsivais, and R. Esquivel-Sirvent, J. Appl. Phys. **89**, 2886 (2001).
[13] M. Spivack, Proc. R. Soc. London, Ser. A **435**, 615 (1991).
[14] A. J. Cooper and D. G. Crighton, Proc. R. Soc. London, Ser. A **454**, 1337 (1998).
[15] W. T. Thomson, J. Appl. Phys. **21**, 89 (1950).
[16] N. A. Haskell, Bull. Seismol. Soc. Am. **43**, 17 (1953).
[17] J. S. Sastry and M. L. Munjal, J. Sound Vib. **182**, 109 (1995).
[18] J. W. Dunkin, Bull. Seismol. Soc. Am. **55**, 335 (1965).
[19] J. M. Orellana and B. Collet, *Proceedings of the Symposium on the Mechanics of Electromagnetic Materials and Structures of the ASME Mechanics and Materials Conference 1929, Blacksburg, VA* (IOS Press, 2000), pp. 124–137.
[20] J. M. Orellana, Ph.D. thesis, University Pierre and Marie Curie (Paris VI) Paris, France, 2001.
[21] B. Collet, Ultrasonics **42**, 189 (2004).
[22] B. Honein, A. M. B. Braga, P. Barbone, and G. Hermann, *Electromagnetic Forces and Applications*, edited by J. Tani and T. Takagi (Elsevier Science Publishers, Amsterdam, 1992), pp. 437–440.
[23] K. A. Ingebrigtsen and A. Tonning, Phys. Rev. **184**, 942 (1969).
[24] J. Lothe and D. M. Barnett, J. Appl. Phys. **47**, 1799 (1976).
[25] J. M. Orellana and B. Collet, *Proccedings of the IUTAM Symposium on Mechanical Waves for Composites Structures Characterization, Greece, 2000* (Kluwer, Dordrecht, 2001), p. 125.
[26] V. Y. Zhang, T. Gryba, J. M. Orellana, and B. Collet, Acta. Acust. Acust. **88**, 218 (2002).
[27] L. Knopoff, Bull. Seismol. Soc. Am. **54**, 431 (1964).
[28] H. Schmidt and G. Tango, Geophys. J. R. Astron. Soc. **84**, 331

(1986).
[29] H. Schmidt and F. B. Jensen, J. Acoust. Soc. Am. **77**, 813 (1985).
[30] A. K. Mal, Wave Motion **10**, 257 (1988).
[31] J. L. Bleustein, Appl. Phys. Lett. **13**, 412 (1968).
[32] Y. V. Gulyaev, JETP Lett. **9**, 37 (1969).
[33] S. Li, J. Appl. Phys. **80**, 5264 (1996).
[34] B. A. Auld, *Acoustic Fields and Waves in Solids. Vols. I, II* (Wiley-Interscience, New York, 1973).
[35] E. Dieulesaint and D. Royer, *Elastic Waves in Solids: Applications to Signal Processing* (Wiley, Chichester, 1980).
[36] C. Maerfeld and P. Tournois, Appl. Phys. Lett. **19**, 117 (1971).
[37] A. N. Darinskii, I. S. Didenko, and N. F. Naumenko, J. Acoust. Soc. Am. **107**, 2351 (2000); **107**, 2447 (2000).
[38] J. Lothe and D. M. Barnett, Phys. Norv. **8**, 239 (1976).
[39] G. Monsivais, R. Rodríguez-Ramos, R. Esquivel-Sirvent, and L. Fernández-Álvarez, Phys. Rev. B **68**, 174109 (2003).
[40] D. J. Griffiths and C. A. Steinke, Am. J. Phys. **69**, 137 (2001).
[41] K. Aki and P. G. Richards, *Quantitative Seismology. Theory and Methods* (Freeman, San Francisco, 1980).
[42] G. Monsivais, F. Garcia-Moliner, and V. R. Velasco, J. Phys.: Condens. Matter **7**, 5491 (1995).
[43] E. P. Wigner, *Group Theory* (Academic Press, New York, 1959).
[44] M. Moshinsky, *Group Theory and the Many Body Problem* (Gordon and Breach, New York, 1966).
[45] N. W. Ashcroft and N. D. Mermin, *Solid State Physics* (Holt, Rinehart and Winston, New York, 1976).
[46] J. Flores, G. López, G. Monsivais, and M. Moshinsky, Ann. Phys. (San Diego) **172**, 156 (1986).
[47] W. L. Mochán, and M. del Castillo-Mussot, Phys. Rev. B **37**, 6763 (1988).
[48] H. Aynaou, V. R. Velasco, A. Nougaoui, E. H. Boudouti, B. Djafari-Rouhani, and D. Bria, Surf. Sci. **583**, 101 (2003).
[49] G. Monsivais, R. Rodríguez-Ramos, and L. Fernández-Álvarez, Ferroelectrics **268**, 233 (2002).
[50] R. Rodríguez-Ramos, G. Monsivais, J. A. Otero, H. Calás, V. Guerra, and C. Stern, J. Appl. Phys. **96**, 1178 (2004).
[51] G. H. Wannier, Phys. Rev. **117**, 432 (1960); Rev. Mod. Phys. **34**, 645 (1962); *Elements of Solid State Theory* (Cambridge University Press, Cambridge, England, 1959), pp. 190–193.
[52] E. E. Mendez, F. Angulló-Rueda, and J. M. Hong, Phys. Rev. Lett. **60**, 2426 (1988).